JANUARY 2008

SOLAR DESALINATION OF BRACKISH WATER USING MEMBRANE DISTILLATION PROCESS

WRRI Technical Completion Report No. 342

Shuguang Deng

NEW MEXICO WATER RESOURCES RESEARCH INSTITUTE
MSC 3167
New Mexico State University
Box 30001
Las Cruces, New Mexico 88003-0001
Telephone (575) 646-4337 FAX (575) 646-6418
email: nmwrri@wrri.nmsu.edu

SOLAR DESALINATION OF BRACKISH WATER USING MEMBRANE DISTILLATION PROCESS

By

Shuguang Deng
Principal Investigator
Department of Chemical Engineering
New Mexico State University

TECHNICAL COMPLETION REPORT

Account Number 109468

January 2008

New Mexico Water Resources Research Institute

in cooperation with the

Department of Chemical Engineering
New Mexico State University

The research on which this report is based was financed in part by the U.S. Department of the Interior, Geological Survey, through the New Mexico Water Resources Research Institute.

DISCLAIMER

The purpose of the Water Resources Research Institute technical reports is to provide a timely outlet for research results obtained on projects supported in whole or in part by the institute. Through these reports, we are promoting the free exchange of information and ideas, and hope to stimulate thoughtful discussions and actions that may lead to resolution of water problems. The WRRI, through peer review of draft reports, attempts to substantiate the accuracy of information contained within its reports, but the views expressed are those of the authors and do not necessarily reflect those of the WRRI or reviewers. Contents of this publication do not necessarily reflect the views and policies of the Department of the Interior, nor does the mention of trade names or commercial products constitute their endorsement by the United States government.

ABSTRACT

The objective of this research was to evaluate the thermal efficiency of different solar collectors as water heaters and to determine the process parameters of the membrane distillation process using a hollow fiber membrane module for brackish water desalination through experimental and process modeling studies.

It was found from the experimental studies that the Sunearth® flat solar collector had the highest solar to thermal conversion efficiency and a homemade parabolic solar collector had the lowest solar to thermal conversion efficiency.

An experiment of direct contact membrane distillation using hollow fiber membrane module was done to purify brackish water and saline water of high salt content. The salt rejection rate obtained was approximately 99%.

Modeling of heat and mass transfer phenomena associated with the membrane distillation process was also performed. The process parameters like temperature polarization coefficient (TPC), heat transfer coefficient, membrane distillation coefficient (MDC), vapor pressure polarization coefficient (VPC), and permeate stream mass flux have been obtained by modeling calculation. The calculated value of permeate stream flux was then compared with experimental results to check the consistency of the data obtained in this process. The calculated and experimentally obtained mass flux with operating temperature showed a similar behavior, which is desired for an effective direct contact membrane distillation process.

Keywords: Solar collector; direct contact membrane distillation; modeling; temperature polarization coefficient (TPC); heat transfer coefficient; membrane distillation coefficient (MDC); permeate stream water flux

TABLE OF CONTENTS

LIST OF TABLES

LIST OF FIGURES

Figure Page

INTRODUCTION

Membrane distillation is a novel membrane separation process in which two aqueous solutions at different temperatures are separated by a microporous hydrophobic membrane. It involves the transport of feed liquid (hot saline water in desalination process) vapor through the pores of microporous hydrophobic membranes due to the evolved partial vapor pressure. This vapor pressure difference caused by the temperature gradient and concentration difference across the membrane is the main driving force of the process. Of the different configurations of membrane distillation, the direct contact membrane distillation process is described here. The experimental process first has been described, and modeling of heat and mass transfer associated with the process has been done. The experimental and calculated process parameters are analyzed here.

BACKGROUND

Several studies have been done on direct contact membrane distillation (DCMD) process. Lawson et al. [1] measured the permeability parameters associated with the molecular diffusion in DCMD process. The water flux behavior with temperature was studied. Thereby they proposed a dusty gas model of gas transport through porous media to describe the related transport phenomena. Martinez-Diez et al. [2] derived the evaporation efficiency in DCMD. Lagana et al.[3] applied the DCMD technique to produce highly concentrated apple juice using the hollow fiber membrane module. The effect of temperature polarization coefficient and concentration polarization coefficient on the permeate flux were analyzed. A parametric sensitivity analysis of DCMD was proposed by Abu Al-Rub et al. [4]. In this study, parametric sensitivity and the temperature polarization factor were used to study the sensitivity of the mass flux to the different parameters for water production. Ding et al.[5] proposed a new model for mass transfer in direct contact membrane distillation for three types of membranes. Water fluxes at different temperatures and the membrane distillation coefficient (MDC) for each membrane were analyzed from the experiment. Khayet et al.[6] showed the asymmetric polarization in the DCMD process. In this study, the feed and permeate temperature polarization coefficients and the vapor pressure polarization coefficient were defined and analyzed. A new approach to flux enhancement in the DCMD process was done by Cath et al. [7]. The new experimental configuration in this effort provided the reduced temperature polarization coefficients and increased mass transfer of water due to the higher permeability of the membrane used. Khayet et al. [8] proposed a novel modeling of mass transport through a porous membrane (microporous polytetrafluoroethylene and polyvinyledene fluoride membrane) in direct contact membrane distillation. A theoretical model, which considered the pore size distribution with the gas transport mechanisms through the membrane pore, was developed here. A new transport model for DCMD process in laminar flow was discussed by Rodriguez-Maroto et al. [9]. The aim of this study was to apply this model to conventional membrane module and thereby to calculate the differences between the bulk and externally measured temperatures.

Hollow fiber membranes are relatively new, and various research studies are continuing with it. Korngold et al. [10] invented a new desalination process consisting of

air humidification pervaporation through hydrophilic or microporous hydrophobic hollow fibers. The energy requirement for this process also was discussed briefly. Gujit et al. [11] proposed a new model to determine some important membrane properties, such as Knudsen diffusion and viscous flow membrane characteristics, for the hydrophobic (polypropylene, polyethylene) membrane module. A thorough study of microporous polypropylene hollow fiber membranes was done by Kim et al. [12]. Dindore et al. [13] investigated the shell-side mixing of rectangular cross flow hollow fiber membrane contactors using gas phase RTD measurements, thereby measuring the shell-side dispersion coefficient. Sirkar et al. [14] used a new rectangular cross flow hollow fiber membrane module to perform DCMD process for sea water desalination. The great potentiality of the membrane contactors in membrane distillation was discussed by Drioli et al. [15]. A novel composite porous hydrophobic/hydrophobic membrane for DCMD was invented by Khayet et al. [16]. The new membrane developed in this effort is promising for membrane distillation as it creates low resistance to mass flux achieved by the process.

THEORY

Direct contact membrane distillation (DCMD) is the most commonly used and the most effective of the various membrane distillation configurations. Though DCMD is widely used for desalination purposes, it also has been applied for wastewater treatment. In DCMD process, the hydrophobic microporous membrane (hollow fiber membrane in this effort) is in contact with the liquid phase on evaporation and condensation sides of the membrane. The hot and cold liquid streams are in direct contact with both sides of the membrane that has a thickness of b or δ, forming the liquid/vapor interfaces; the liquids flow counter-currently over two sides of the membrane. The vapor evolved from the hot feed is then diffused through the membrane pore and goes to the other side of membrane. It will be condensed by the cold liquid and thus generates permeates. Several theoretical and experimental studies have been published on the DCMD process, and the mechanism of this process can be expressed schematically, as shown in Figure 1 by Abu-Al-Rub et al. [4].

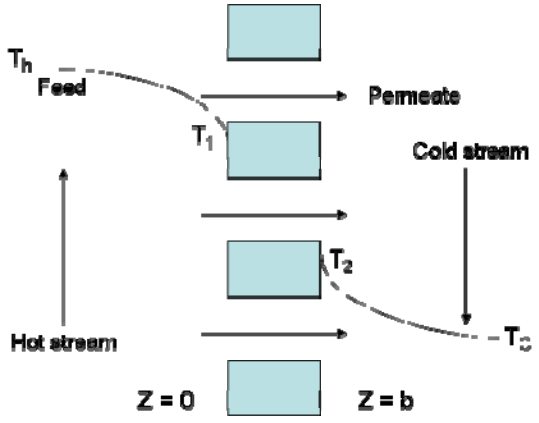

Figure 1. Principle of DCMD

EXPERIMENT

Evaluation of Three Solar Collectors as Water Heaters

Three kinds of solar collectors were used for heating brackish water. They are the Winston series CPC Solargenix® collector shown in Figure 2, the flat plate Sunearth® collector shown in Figure 3, and the homemade parabolic collector shown in Figure 4.

Figure 2. Winston Series CPC Solargenix® Collector

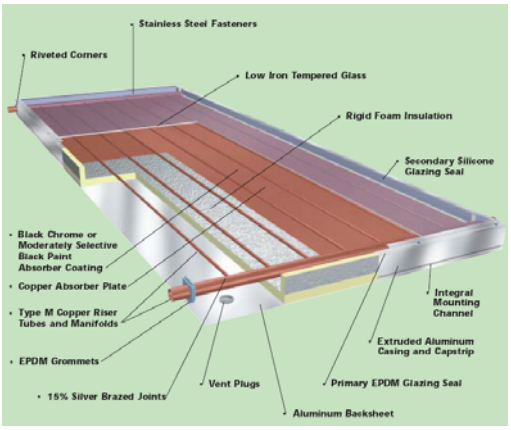

Figure 3. Sunearth® Solar Collector

Figure 4. Homemade Parabolic Collector

The installation conditions of the above mentioned collectors are listed in Table 1. The specifications for all three collectors are given in Tables 2 to 4. The temperatures of the inlet and outlet water were measured with thermocouples, and the water flow rates were measured manually with a graduated cylinder and timer. Each of the collectors was tested independently for conducting analysis to estimate their thermal efficiency. The inlet water temperature for the collectors varied due to the recycling without cooling. Hence, the analysis is based on varied inlet feed water temperature.

Table 1. Installation Condition of Solar Collectors

Location	Las Cruces, NM (NMSU)
Longitude	106.76 W
Latitude	32.34 N
Tilt angle	45
Direction	Facing south
Height from the ground	2.0 m

Table 2. Specifications of CPC Design Solargenix Collectors

Length	2094	mm
Width	1065	mm
Height	863	mm
Gross area	2.23	m^2
Aperture area	2.07	m^2
Number of flow tubes	12	
Tube O.D	22.2	mm
Collector frame	Extruded Aluminum	
Back plate	Aluminum sheet	
Insulation	Polyurethane foam	
Insulation K-factor	0.0024	W/m^oC
Absorber coating	Black crystal	
Reflector	High Quality Aluminum	
Flow tubes	Copper	
Covering plate	Tempered low iron glass	
Thickness of covering plate	3.3	mm
Dimensions of covering plate	12.61 x 25.01	m
Absorption rate	97	%
Emissivity	0.12	
Emittance ratio	7	%
Transmissivity	90.1	%

Table 3. Specifications of Flat Plate Sunearth Model EP-40 Solar Collector

Length	3.1	m
Width	1.22	m
Height	0.08	m
Gross area	3.79	m^2
Aperture area	3.47	m^2
Number of flow tubes	7	
Collector frame	Anodised Aluminum	
Back plate	Textured Aluminum	
Absorber coating	Black paint	
Glazing	Tempered low iron glass	
Insulation	Polyisocyanurate	
Flow tubes	Type m copper	
Covering plate	Low iron tempered glass	
Thickness of covering plate	3.175	mm
Transmissivity (t)	0.90	
Heat removal factor (Fr)	0.8	
Overall heat transfer coefficient (U)	5	$W/m^2.K$
Absorption rate (Alpha)	0.97	

Table 4. Specification of Homemade Paraboloidal Trough Collector

Collector type	Paraboloidal troughs	
Length	47	mm
Width	242	mm
Height	0.08	m
Gross area	2.35	m^2
Aperture area	2.27	m^2

Membrane Specifications

A shell and tube hollow fiber membrane contactor has been applied in this work, and it is obtained from Liqui-Cel (Membrana). The membrane contactor is a hollow fiber shell and tube membrane contactor. This geometry allows a large contact area with a minimum volume requirement. This module exhibits counter-current flow configuration. The hot feed liquid here will be carried through the lumen side, whereas the cold liquid will flow through the shell side of the module counter-currently. The hot vapor (from hot liquid of the lumen side) is diffused through the hydrophobic membrane pore and enters in the shell side. The vapor is then condensed in the shell side by the cold fluid and generates permeate. The cumulated volume of the tubing and fiber side of the membrane module is equal to 0.5 liter, whereas the volume for the shell side and the tubing is equal to 0.25 liter (according to Baudot et al. [17]).The schematic design of this membrane module is shown in Figure 5. Membrane specifications are given in Table 5.

Figure 5. Hollow Fiber Membrane Contactor (Liquicell Extra Flow)

Table 5. Characteristics of hollow fiber membrane contactors [17]

Provider:	Celgard
Model:	Liquicell-Extraflow
Contactor type:	Shell and tube
Membrane type:	Hollow fiber
Overall contact area:	1.4 m^2
Fiber material/type:	Polypropylene (PP) (X-30)
Number of fibers:	9,950
Outer fiber diameter:	300 μm
Fiber wall thickness:	30 μm
Fiber porosity:	0.40
Pore tortuosity:	2.25
Pore diameter:	0.03 μm

Membrane Distillation Experimental Steps

- Feed brackish water and cold DI water are kept in two tanks called "Feed" and "Permeate or distillate". The feed brackish water is heated up to 80-90°C by a water heater immersed into the feed tank, and the cold DI water is cooled up to 8-10°C by a chiller (Water bath – Isotemp 3006S).
- The heated water is carried out to the membrane module by a centrifugal pump, and the cold water is also pumped to the membrane module by another centrifugal pump.
- Four thermocouples are connected to measure the temperatures accurately at the feed (hot and cold), permeate, and concentrated brine sides.
- Four pressure gauges have been installed, one in each line to measure the system pressures.
- Digital flow meters are then placed in each line (hot feed, cold feed, permeate, and concentrated brine line) to measure the liquid flow accurately.

- The heated feed is passed through the lower chamber of the membrane module, and the cold DI water is carried out through the upper chamber of the module counter-currently.
- The vapor generated from the heated water then diffuses through the membrane pore, and it will enter in the upper chamber of the module.
- The vapor is condensed by the cold water in this upper chamber, and produced fresh water will go out as distillate/permeate from the module.
- This fresh water is recycled to the permeate tank, and the concentrated brine is returned to the hot water tank.
- The process is continued over a long time (around eight hours), and the experimental data are collected and characterized thereafter.
- The total process line, tube, and equipment are insulated thoroughly to get optimum heat transfer.

The experimental procedure is shown schematically in Figure 6.

Figure 6. A Complete View of DCMD Application by Using Hollow Fiber Membrane Module

The salt rejection in this experiment is over 99 %, and it gives an impression that the process is an extremely effective one for desalination purpose.

MODELING OF HEAT AND MASS TRANSFER PHENOMENA

Modeling is most important for designing a proper and effective DCMD process. The calculation of various parameters evolved from heat and mass transfer phenomena of membrane distillation can be done through proper modeling. The parameters like process efficiency, heat transfer coefficient, mass transfer coefficient, temperature polarization, vapor pressure polarization, concentration polarization, and so on can be derived from a complete modeling. Therefore, it can give the clear idea about the performance of the MD process. A complete modeling of the membrane distillation process using the flat sheet membrane module as well as the hollow fiber membrane module is derived. Heat and mass transfer phenomena through the hydrophobic microporous membrane in the DCMD process are shown schematically in Figure 7.

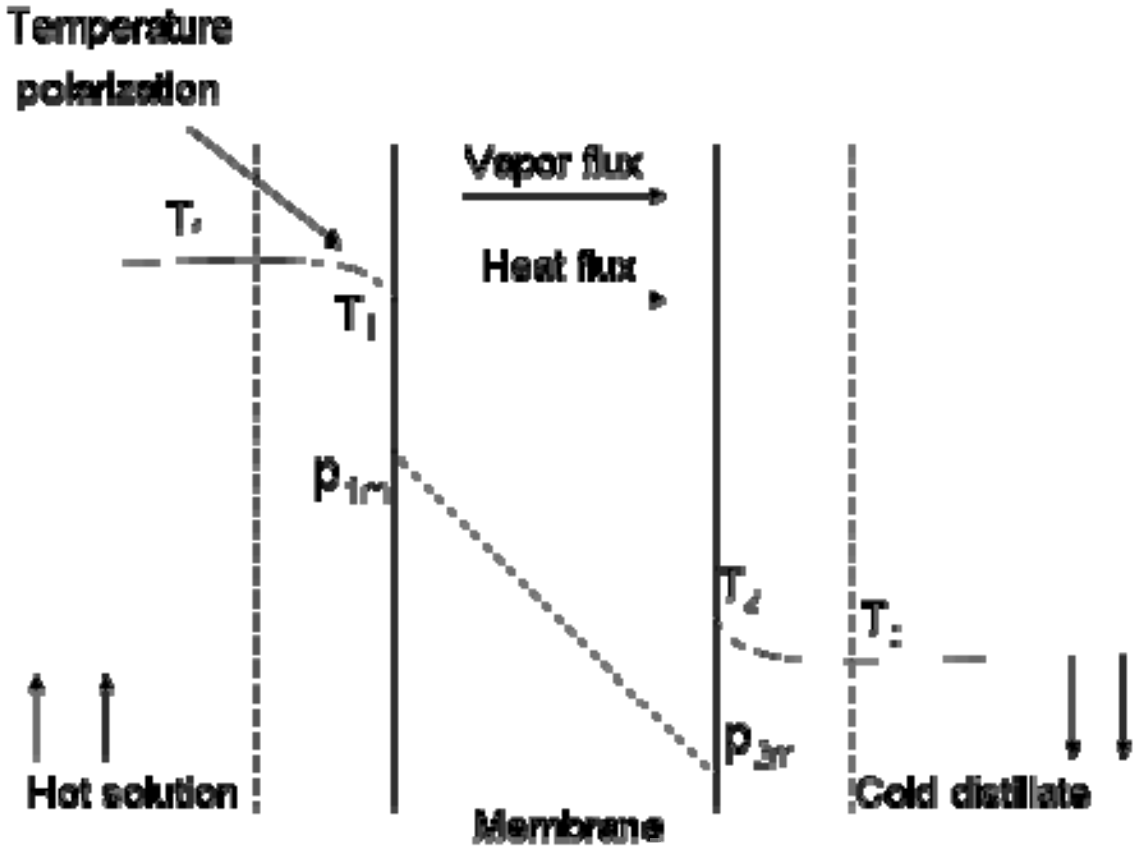

Figure 7. Temperature and Vapor Pressure Profiles [14]

Heat Transfer Phenomena

Thermal energy is first transferred from the hot feed (hot brackish/saline water) across the thermal boundary layer to the membrane surface. Liquid is vaporized at the boundary of the feed, and heat is then transferred to the membrane via mass transfer. The

vapor goes to the upper section of the module where the cold water is flowing counter-currently.

Bulk temperature cannot be considered as the externally measured temperature due to some factors. The measured temperatures can be considered as bulk temperatures at the inlets of hot and cold water flow channels. However, the measured temperatures of the outlets of the membrane module cannot be assumed to be bulk temperature, since it is the average temperature at the outlets of the membrane module that will differ significantly from the bulk temperatures at the outlets of the module. Interfacial membrane temperatures are the most important while modeling the heat transfer in the DCMD process. The heat transfer model described here is built on the published work of Abu Al-Rub et al. [4].

The total heat transfer phenomena can be expressed in three different zones of interest:

- The heat transfer from bulk feed to the membrane surface
- Heat transfer through the membrane
- The heat transfer from the cold side of the membrane to the coolant fluid

The heat transfer from bulk feed to the membrane surface can be expressed as:

$$Q = h_f(T_f - T_1) \quad (1)$$

where h_f is the convective heat transfer coefficient in the hot feed side and T_h and T_1 are the hot feed and membrane surface temperatures, respectively.

Heat transfer through the membrane is expressed as:

$$Q = \frac{K_m}{\delta}(T_1 - T_2) + N\lambda + NC_{pg}(T_1\text{-}T_2) \quad (2)$$

where K_m is the effective thermal conductivity of the membrane, δ is the membrane thickness, N is the permeate/condensate flow rate, λ is the latent heat of water, and C_{pg} is the heat capacity of water. The third term represents the sensible heat which is negligible in comparison with the other two terms.

$$K_m = \varepsilon Kg + (1\text{-}\varepsilon)Ks \quad (3)$$

Heat is also conducted through the membrane pore. The hot vapor is then condensed with the presence of cold water. So heat finally is transferred to the cold water. This conductive heat transport across this membrane can be treated as inefficiency because this heat is no longer available for use in evaporation.

The heat transfer from the cold side of the membrane to the coolant fluid is given as:

$$Q = h_c(T_2 - T_c) \quad (4)$$

Heat flux from hot feed water to the cold water can be expressed as:

$$Q = h_f(T_f - T_1) = \frac{K_m}{\delta}(T_1 - T_2) + N\lambda \;\; = \; h_c(T_2 - T_c) \tag{5}$$

where

$$T_1 = \beta\left\{\left(1 + \frac{K_m}{h_c\delta}\right)T_f + \left(\frac{K_m}{h_h\delta}\right)T_c - \frac{N\lambda}{h_h}\right\} \tag{6}$$

$$T_2 = \beta\left\{\left(1 + \frac{K_m}{h_h\delta}\right)T_c + \left(\frac{K_m}{h_c\delta}\right)T_h - \frac{N\lambda}{h_c}\right\} \tag{7}$$

where

$$\beta = \frac{1}{\left(1 + \frac{K_m}{h_h\delta} + \frac{K_m}{h_c\delta}\right)} \tag{8}$$

The main driving force for transmembrane mass transfer highly depends on the temperature difference between the evaporation and condensation surfaces which, is (T_1-T_2).

From the previous work of Khayet et al. [6], the estimation of heat transfer for the hollow fiber membrane module has been derived. It considers the same equation described above for calculation, but it needs some more approximation, which is described below. To determine T_1 and T_2 from the above Equations (6) and (7), h_f and h_c need to be found, and it can be determined from the Nusselt number in the following ways:

For feed circulating in the lumen side of the membrane module under Laminar flow regimes:

$$Nu = \frac{h_f d_h}{k} = 1.86\left(\mathrm{Re}\,\mathrm{Pr}\,\frac{d_h}{L}\right)^{1/3} \tag{9}$$

For Transitional flow:

$$Nu = \frac{h_f d_h}{k} = 0.116\left(\mathrm{Re}^{2/3} - 125\right)\mathrm{Pr}^{1/3}\left[1 + \left(\frac{d_h}{L}\right)^{2/3}\right] \tag{10}$$

For Turbulent flow:

$$Nu = \frac{h_f d_h}{k} = 0.023\,\mathrm{Re}^{4/5}\,\mathrm{Pr}^{0.4} \tag{11}$$

For the permeate circulating in the shell side of the module, parallel and cross flow will occur simultaneously, and in this case, the Kreith and Bohn [19] correlation should be used:

$$Nu = \frac{h_f d_h}{k} = 0.206\left(Re\cos\alpha\right)^{0.63} Pr^{0.36} \tag{12}$$

where α = yaw angle and varies between 0° (for pure cross flow) to 90° (for pure parallel flow).

Overall heat transfer coefficient:

$$H = \left[\frac{1}{h_f} + \frac{1}{(\varepsilon K_g + (1-\varepsilon)K_s)/\delta + N\lambda/(T_1 - T_2)} + \frac{1}{h_c}\right]^{-1} \tag{13}$$

Overall heat transfer coefficient is valid for the hot feed and cold permeate phase:

$$h = \frac{h_f h_c}{h_f + h_c} \tag{14}$$

Temperature Polarization

The ratio of useful energy for mass transfer of vapors to the total energy involved in the process is called the temperature polarization coefficient (TPC). This work has been taken from the previous study of Khayet et al [6]. It is the fraction of total thermal driving force that contributed to mass transfer, and it is expressed as:

$$\tau = \frac{(T_1 - T_2)}{(T_f - T_c)} = 1 - \frac{H}{h} \tag{15}$$

The evaporation rate will be increased (so the mass flux will be increased) if difference between T_f and T_1 and between T_2 and T_c will increase. Therefore, the difference between T_1 and T_2 should be as high as possible.

The temperature polarization coefficient generally is estimated by the assumption that its value is the same at both membrane sides. So it assumes that there are equal feed and permeate heat transfer coefficients. But in reality, heat transfer at each side of the membrane should be different by depending upon the temperature and type of solutions. As a consequence, the temperature polarization coefficient of each phase will be different. This result is an asymmetric temperature profile.

Equations (14) and (15) can be rearranged as:

$$\tau = \tau_f + \tau_c - 1 \tag{16}$$

where τ_f = Temperature polarization coefficient corresponding to feed

τ_c = Temperature polarization coefficient corresponding to permeate

$$\tau_f = 1 - \frac{H}{h_f} = \frac{T_l - T_c}{T_f - T_c} \quad (17)$$

$$\tau_c = 1 - \frac{H}{h_c} = \frac{T_f - T_2}{T_f - T_c} \quad (18)$$

Two factors influencing the temperature polarization are:

a) If there is large heat transfer through the feed and permeate, the temperatures at the membrane surfaces approach the corresponding bulk phase temperature. So the temperature polarization coefficient τ_f and τ_c and τ will be in unity [according to Equation (16)].
b) If both the feed and permeate heat-transfer coefficient are small, then the difference between the temperatures at membrane surfaces and that of bulk phases will be large. So the temperature polarization approaches zero [Equation (15)]. In this case, the temperature polarization effects are very important, and the heat transfer resistances of the boundary layers control the DCMD process.

Mass Transfer Phenomena

In this system, mass transfer occurs through a microporous hydrophobic membrane. The hot and cold fluids flow tangentially and counter-currently to the membrane surface through the installed hollow fiber membrane module. The driving force for mass transfer is the temperature difference. This difference will result in a water vapor pressure difference and produce water flux through the membrane. The heat required for water evaporation at the membrane-liquid interface comes from the hot liquid phase. Similarly, the condensation takes place at the other membrane-liquid interface, and heat can be removed by the cold liquid phase adjacent to it. Also the flux generated through the membrane surface creates a temperature gradient along the flow direction (x-coordinate). The temperature profile is shown in Figure 21. Mass transfer in the DCMD process takes place in certain steps. The membrane exerts its influence on transmembrane water flux in the following three ways:

1) The water molecules move through the pores only of the membrane, so the effective area of mass transfer is less than the total membrane area,
2) Usually the membrane pore structure does not go straight through the membrane, so the path of vapor transport is greater than the thickness of the membrane, and
3) The momentum of the vapor molecules in the membrane pore is usually decreased; the resistance to diffusion increases.

The mass transfer process in the DCMD includes two steps:

1) The vaporization of hot liquid at liquid/vapor interface and the mass transfer resistance within the concentration boundary layer on the hot side of the membrane.
2) The vapor then passes through the microporous hydrophobic membrane.

Determination of Overall Flux of Water Vapor

For mass transfer through the membrane, an empirical approach has been derived (Rodriguez-Maroto et al. [9]).

The overall flux of water vapor for the complete membrane module can be written as:

$$N = \frac{1}{L}\int_0^L N(x)dx \tag{19}$$

The mass flux is proportional to the vapor pressure difference across the membrane, and it can be expressed as:

$$N(x) = C(x)\left[p_1(T_1) - p_2(T_2)\right] \tag{20}$$

where C(x) = Membrane distillation coefficient (MDC)
$p_1(T_1)$, $p_2(T_2)$ = Vapor pressure of water at the membrane surface = f(temperature at the membrane interface).

There is no convenient process to measure the water vapor pressures within the membrane mentioned in Equation (20). So, it should be measured in terms of the temperatures. According to Khayet et al. [8], for low values of transmembrane bulk temperature difference, the following expression can be used:

$$N(x) = C(x)\left(\frac{dp}{dT}\right)_{Tav}\left(T_1 - T_2\right) \tag{21}$$

T_{av} = Average temperature along the pores where

$$T_{av} = \frac{T_1 + T_2}{2} \tag{22}$$

(dp/dT) can be evaluated from the Clausius-Clapeyron equation and the Antoine equation to calculate vapor pressure:

$$\left(\frac{dp}{dT}\right)_{Tav} = \left[\frac{\Delta H_v}{RT^2}\exp\left(23.238 - \frac{3841}{T - 45}\right)\right]_{Tav} \tag{23}$$

$p_1(T_1)$ and $p_2(T_2)$ can be derived by using the Antoine equation:

$$p_i = \exp\left(23.238 - \frac{3841}{T_i - 45}\right), \quad i = 1,2 \tag{24}$$

So substituting the Equations (20), (21), (22), (23), (24) into Equation (19), the total water flux can be calculated by the following equation:

$$N(x) = C(x)\left[p_1(T_1) - p_2(T_2)\right] \tag{25}$$

Determination of Membrane Distillation Coefficient

Considering the dusty gas model for gas transport through porous media, the vapor transport through the membrane pores takes place by the combination of Knudsen and molecular mechanisms [9] explained above, and that can be expressed as:

$$C(x) = \frac{N}{\Delta P_v} = \frac{\varepsilon}{\tau\delta}\frac{M}{RT_{av}}\left(\frac{1}{D_k} + \frac{P_a}{PD_d}\right)^{-1} \tag{26}$$

The values PD_d(Pa/m^{2}s) of Equation (26) for water vapor are given (Bird et al. [18]) by:

$$PD_d = 4.46T_{av}^{2.334}10^{-6} \tag{27}$$

D_k can be expressed as:

$$D_k = \frac{2\varepsilon r}{3\tau}\left(\frac{8RT_{av}}{\pi M}\right)^{1/2} \tag{28}$$

D_d can be expressed as:

$$D_d = \frac{\varepsilon}{\tau}PD \tag{29}$$

where D_k = Knudsen diffusion coefficient of water
D_d = Diffusion coefficient of water vapor in air
P_a = Air pressure entrapped in the pores
M = Molecular weight of water
R = Gas constant
P = Total pressure inside the pores. It is equal to the static pressure above the liquid in the feed and permeates in the tank and can be considered as atmospheric pressure. So P is equal to the sum of P_a and the water vapor pressure within the pores.
D = Water diffusion coefficient

After getting the values from the above equation, the water flux for the DCMD process, employing the flat-sheet membrane module can be derived by using Equations (25), (26), (27), (28), (29):

$$N(x) = C(x)\left[p_1(T_1) - p_2(T_2)\right] \tag{30}$$

The value of C(x) can be obtained from the following equation:

$$C(x) = \frac{\varepsilon}{\tau\delta}\frac{M}{RT_{av}}\left(\frac{1}{D_k} + \frac{P_a}{PD_d}\right)^{-1}$$

Vapor Pressure Polarization Coefficient (VPC)

In practical application, the driving force for the mass transfer will be decreased because of the presence of boundary layers adjoining both faces of the membrane. So there will be a distinct difference between the transmembrane pressure difference (ΔP_v) and that in the bulk phase (ΔP_{vb}). Therefore, Equation (26) cannot be used directly. In that case, the vapor pressure polarization coefficient (η) should be introduced, which is expressed as:

$$\eta = \frac{\Delta P_v}{\Delta P_{vb}} = \frac{C_b}{C} \tag{31}$$

where C_b is the global membrane distillation coefficient.

The vapor pressure polarization coefficient is then defined as:

$$\eta = \eta_f - \eta_c - 1 \tag{32}$$

where η_f = Vapor pressure polarization coefficient in the feed
η_c = Vapor pressure polarization coefficient in the permeate

Analogous to the temperature polarization coefficient [defined in Equations (17) and (18)], the above vapor pressure polarization coefficients (η_f and η_c) can be expressed (Khayet et al. [6]) as:

$$\eta_f = \frac{P_v(x_1, T_1) - P_v(T_c)}{P_v(x_f, T_f) - P_v(T_c)} \tag{33}$$

$$\eta_c = \frac{P_v(x_f, T_f) - P_v(T_2)}{P_v(x_f, T_f) - P_v(T_c)} \tag{34}$$

where x_f, x_1 = Molar solute concentrations in the bulk feed and at the feed membrane surface respectively.
x_c, x_2 = Molar solute concentrations in the bulk permeate and at the permeate membrane surface respectively.

Again $P_v(x,T)$ can be defined as:

$$P_v(x,T) = a(x,T)P_v^{\,0}(T) \tag{35}$$

where a(x,T) = The water activity in the salt aqueous solution
P_v^0 (T) = Vapor pressure of distilled water

Vapor pressure of distilled water can be determined from the Antoine equation:

$$P_v^{\ 0} = \exp\left(23.238 - \frac{3841}{T_c - 45}\right) \tag{36}$$

RESULTS AND DISCUSSION

Efficiencies of Solar Collectors

The solar data collected in this project are summarized in Table 6. The thermal efficiency of the three solar collectors is in the order of Sunearth® > Soalrgenix® > Homemade parabolic collector.

Table 6. Solar Data of Three Collectors

Panel Type	Time	T (K)		ΔT (K)	Mass flow rate (Kg/hr)	Solar energy-SUNY Glo (Wh/m^2)	Area of the Collector (m^2)	ΔT/Ht	Efficiency (%)
		Inlet	Outlet						
CPC Solargenix collector	11:00	380	387	7	7.46	928	8.28	0.0075	32.80
	12:00	400	409	9	7.46	990	8.28	0.0091	32.77
	13:00	418	428	10	7.46	1009	8.28	0.0099	32.76
	14:00	426	436	10	7.46	950	8.28	0.0105	32.75
	15:00	427	437	10	7.46	827	8.28	0.0121	32.73
	16:00	421	428	7	7.46	568	8.28	0.0123	32.74
New flat plate Solarearth collector	10:00	364	365	1	7.46	829	3.791	0.0012	70.23
	11:00	373	386	13	7.46	953	3.791	0.0136	64.35
	14:00	387	420	33	7.46	1014	3.791	0.0325	55.41
	15:00	385	420	35	7.46	1009	3.791	0.0347	54.39
	16:00	383	416	33	7.46	950	3.791	0.0347	54.37
Paraboidal trough collector	13:00	317	318	1.26	7.46	1009	2.278	0.0012	0.44
	14:00	318	321	3.48	7.46	980	2.278	0.0036	1.26
	15:00	319	320	1.25	7.46	833	2.278	0.0015	0.53
	16:00	313	319	6.11	7.46	479	2.278	0.0128	4.52
	17:00	311	316	5.00	7.46	334	2.278	0.0150	5.30

The homemade parabolic collector was found to have the lowest efficiency of less than 5%. The thermal efficiency of this collector increased with solar exposure time due to increased solar irradiation as shown in Figure 8, and the efficiency decreased with increase in inlet water temperature as shown in Figure 9.

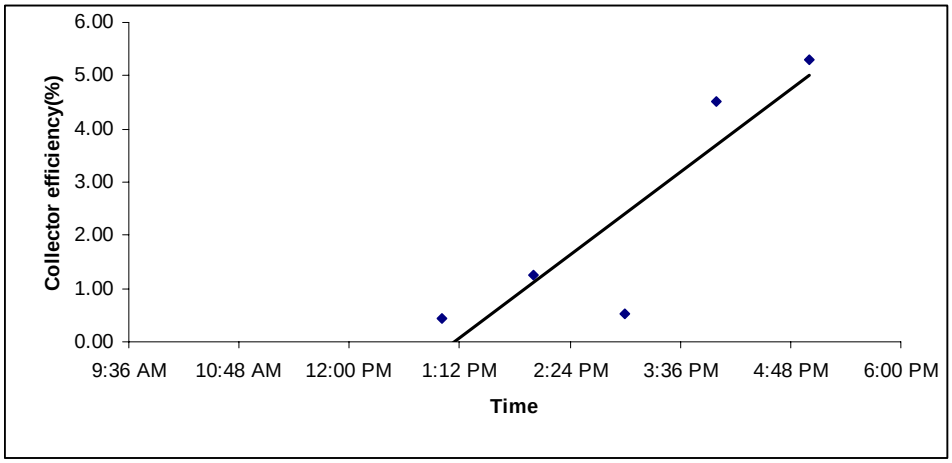

Figure 8. Variation of Homemade Paraboloidal Trough Solar Collector Efficiency with Irradiation Time

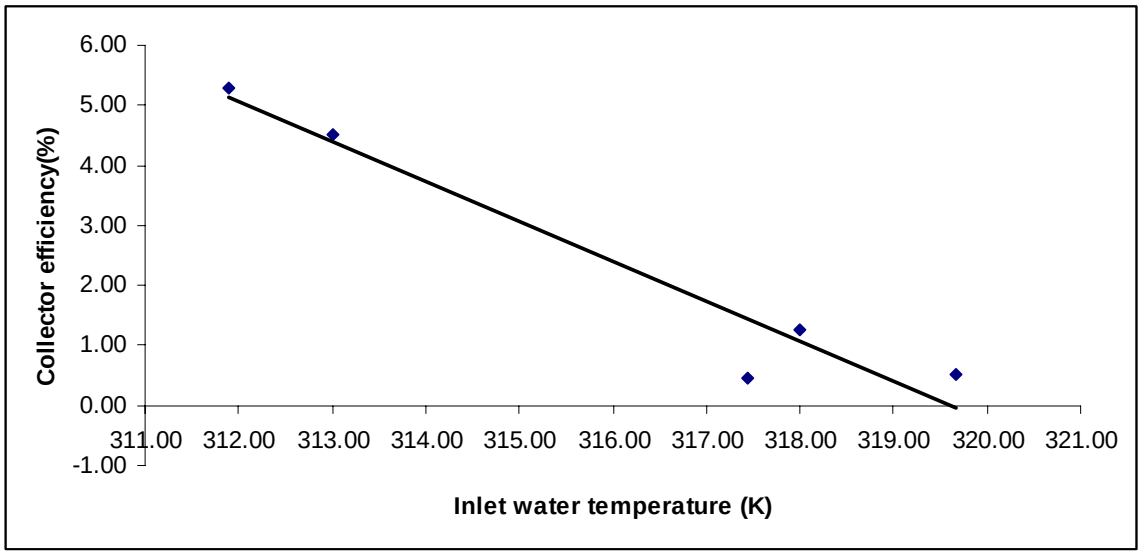

Figure 9. Variation of Paraboloidal Trough Collector Efficiency with Inlet Water Temperature

The obvious reason for the low efficiency of the homemade paraboloidal trough collector is due to lack of proper insulation and a cover glass to retain the heat absorbed by the collector. Hence this collector is least suitable for coupling with a membrane distillation unit.

A representative efficiency variation with time is plotted in Figure 10. The efficiency of Solargenix® collector fluctuated around 32.75% and decreased slightly with time. The decrease in efficiency with time is attributed to increased inlet water temperature that reduces the collector efficiency as shown in Figure 11. This is basically because the heat transfer driving force (temperature difference between the collector and inlet water) decreases with increasing inlet water temperature. Certainly the weather conditions, including sunshine, wind, and cloud coverage, have a strong effect on the solar collector efficiency test results.

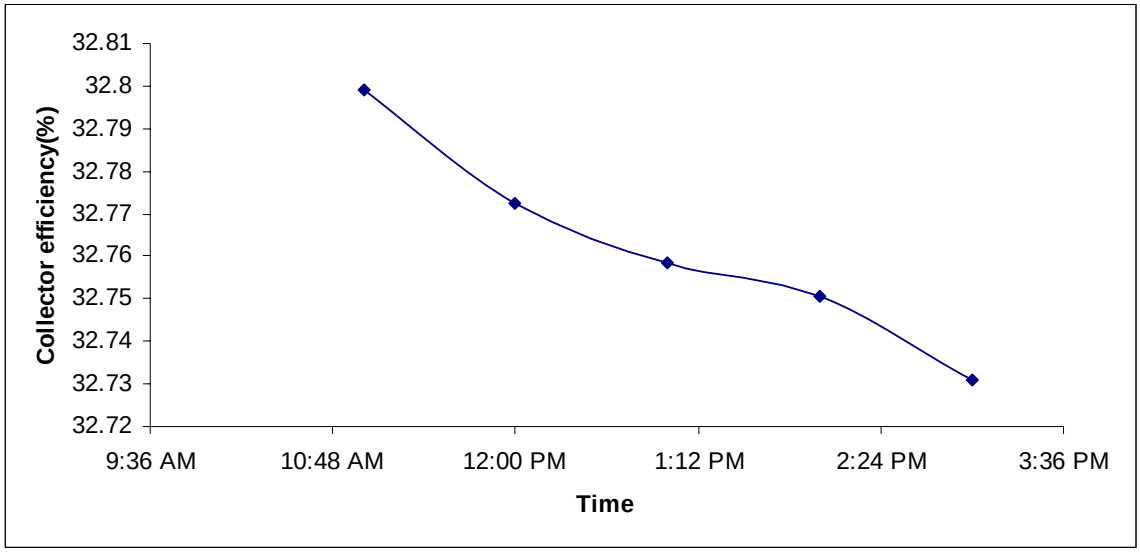

Figure 10. Variation of CPC Solargenix Collector Efficiency with Time

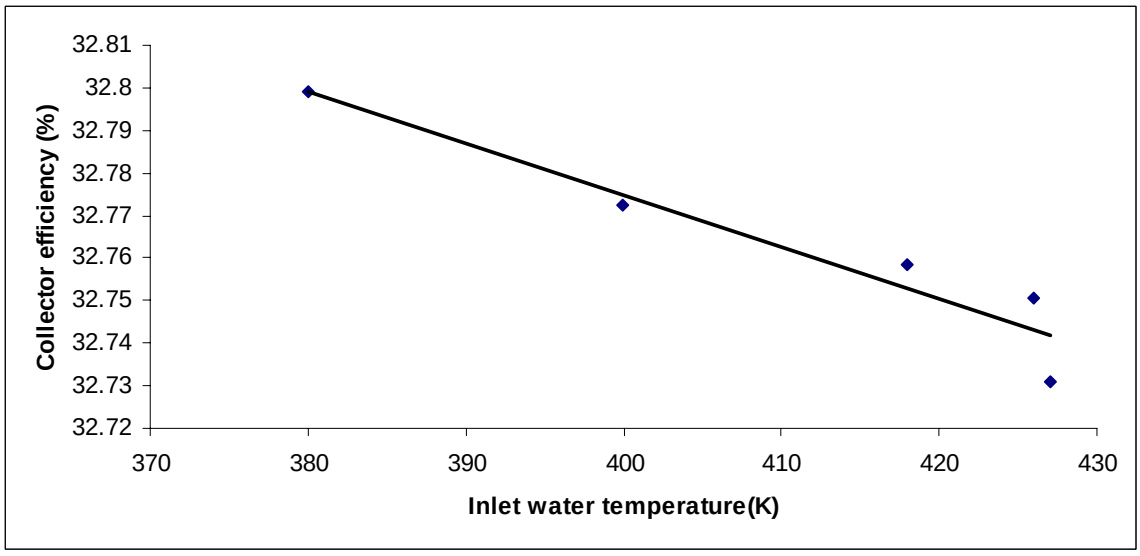

Figure 11.Variation of CPC Solargenix Collector Efficiency with Inlet Water Temperature

Among the three collectors taken for analysis, the Sunearth® flat plate collector has the highest collector efficiency with a maximum of 70% percent. The minimum efficiency value recorded was 54%. The efficiency value was found to decrease with time and increase in inlet water temperature. This could be attributed to the fluctuation in solar irradiation value. Figure 12 and Figure 13 show the collector efficiency variation with time and inlet water temperature.

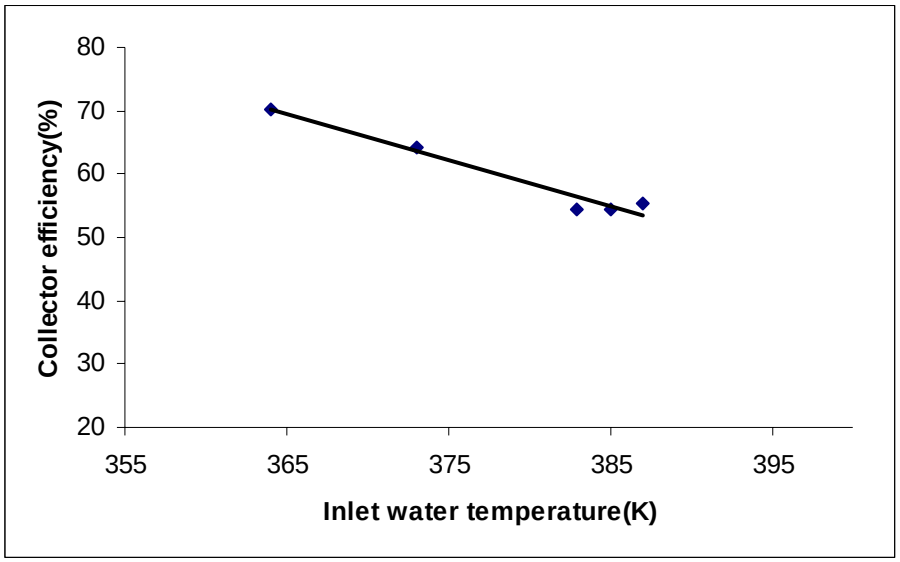

Figure 12. Variation of Sunearth® Flat Plate Collector Efficiency with Inlet Water Temperature

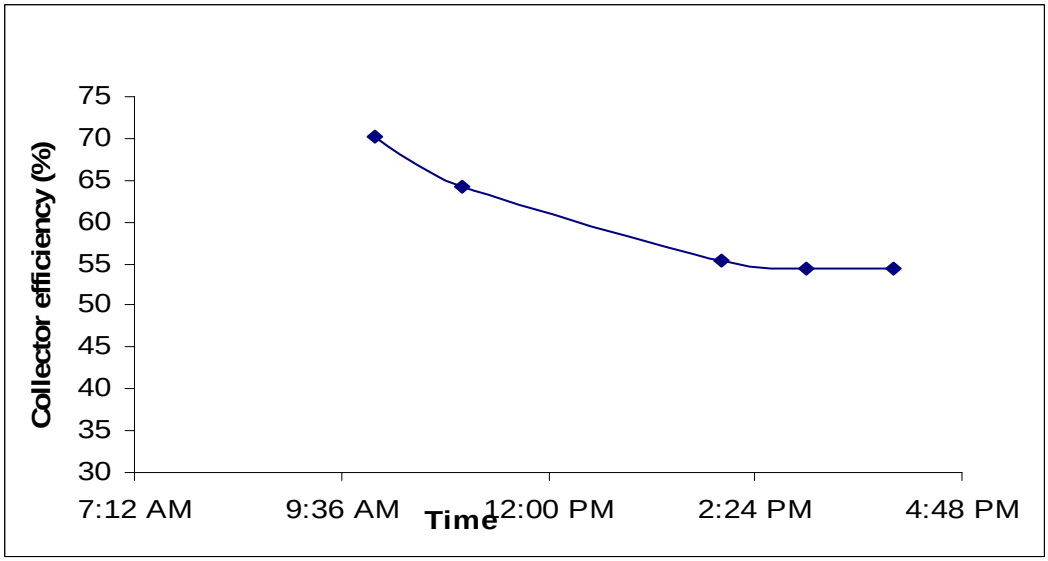

Figure 13. Variation of Sunearth® Flat Plate Collector Efficiency with Time

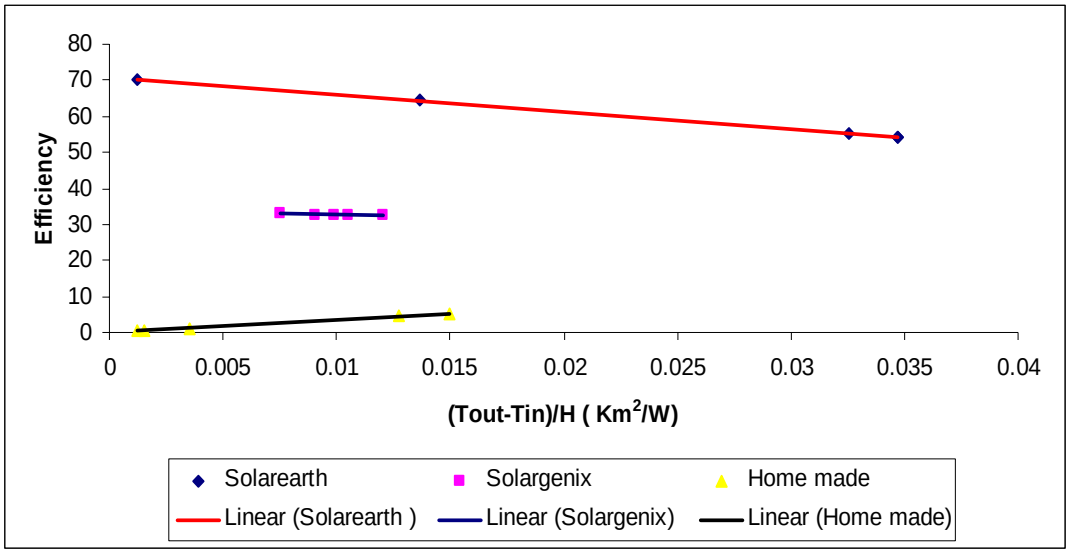

Figure 14. Efficiency of Different Collectors

A graph is drawn between efficiency versus ΔT/ H. The Sunearth® collector efficiency decreases with an increase in (ΔT/ H) value. The efficiency of Solargenix® and the paraboloidal collector remains constant with an increase in (ΔT/ H). The use of the Sunearth® collector seems more compatible for use with the membrane distillation process due to high efficiency.

The weather plays an important role in solar energy harnessing. It can be studied by analyzing the value of clearness index, which is the ratio of terrestrial insolation to that of extraterrestrial insolation. The clearness index varies from 0.50 to 0.73 for Las Cruces from 2003 to 2005. From Figure 15, the maximum attenuation can be seen.

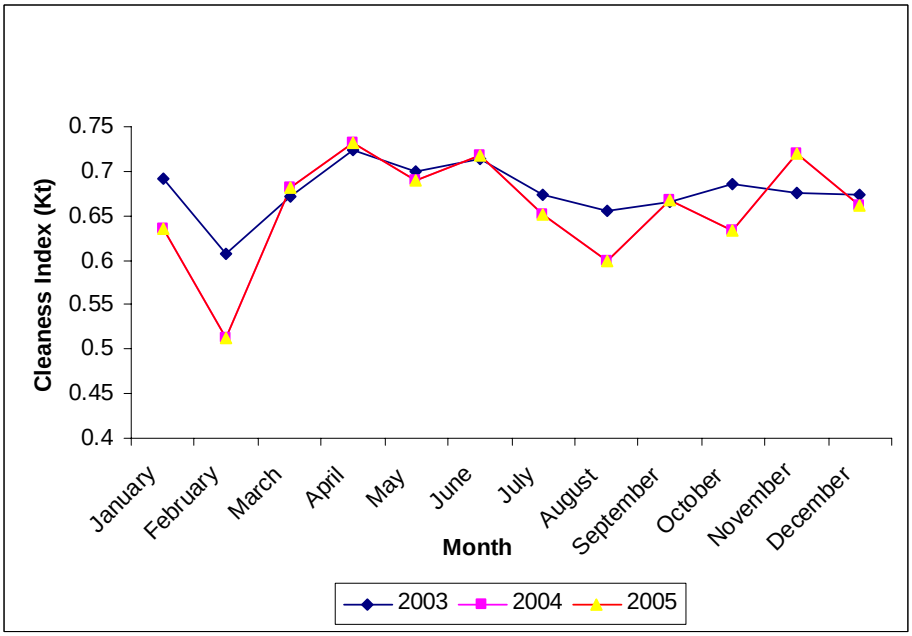

Figure 15. Variation of Clearness Index with Month for Las Cruces from 2003 to 2005

This shows that the atmospheric condition does not greatly attenuate solar radiation. This result demonstrates that use of solar energy for membrane distillation is reliable in Las Cruces and use of high efficiency collectors would impart the required energy to maintain the feed water temperature from 60 to 80^{o}C, which is the operating temperature required for the membrane distillation process.

For all calculation purposes, solar insolation values for 2006 were approximated to the values published for the year 2005 by NSRD. This was approximated based on the graph drawn for solar insolation values for the years 2001 to 2005. It can be seen from Figure 16 that the values remains almost the same for a given month.

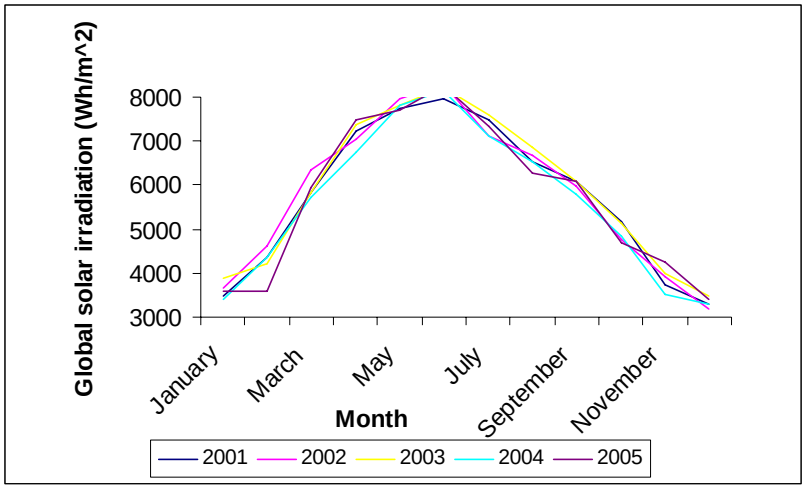

Figure 16.Variation of Global Irradiation by the Month for Las Cruces from 2001 to 2005

In summary, three different kinds of solar collectors were taken for analysis to determine their efficiencies. The Sunearth® solar collector has the highest efficiency, and thus it can be effectively used for heating feed water for the membrane distillation process. Future work can be carried out in testing the collector efficiencies at a steady state condition and at constant inlet feed water temperature to acquire more accurate results and conclusions. This research should be considered as a stepping stone towards using solar energy for a membrane distillation process. Research can be carried out in various areas, such as design and economic, for a solar powered water desalination process.

Temperature Polarization Coefficient (TPC)

Temperature polarization coefficient has been determined from the derived modeling. The behavior of the temperature polarization with the bulk temperature difference has been given in the Figure 17.

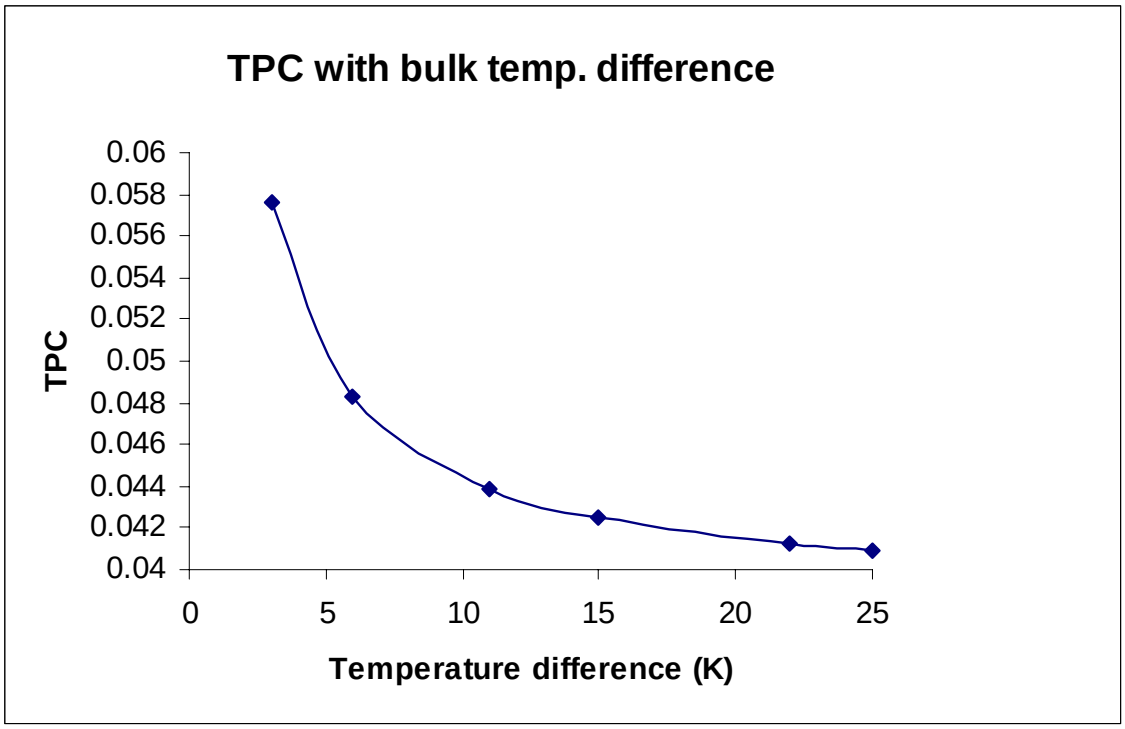

Figure 17. Overall TPC with Bulk Temperature Difference

From the graph, it is understood that with an increase in temperature difference, TPC decreases, which is desired for the process. The range of TPC is between 0.04 to 0.06, which is desired level.

Overall Heat Transfer Coefficient

In Figure 18, the behavior of the heat transfer coefficient with the increase of operating temperature has been shown. With an increase of the operating temperature difference, the heat transfer should increase. But in practice, it is not possible to restrain all the heat in the module. So some heat will be lost. Since the insulation of the experimental process described here is in good condition, heat loss is minimized. So the heat transfer coefficient is nearly constant over the wide temperature region.

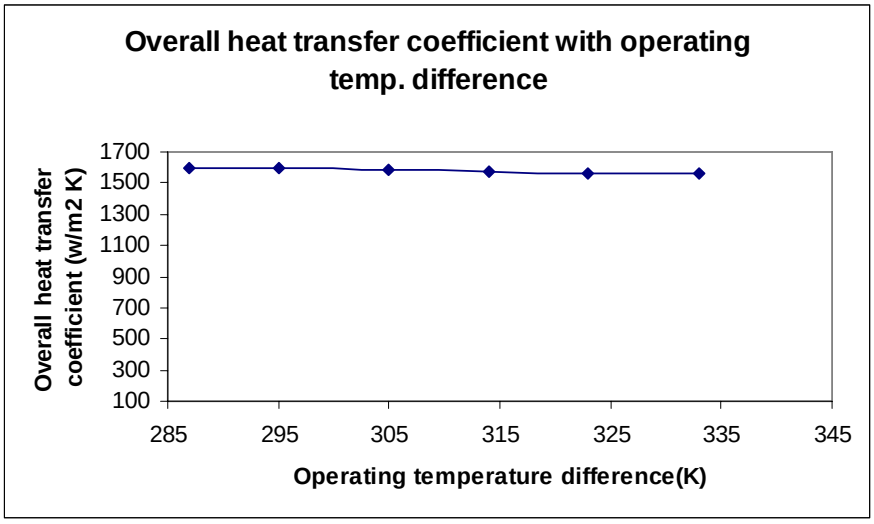

Figure 18. Overall Heat Transfer Coefficient with Operating Temperature Difference

The figure demonstrates that overall the heat transfer coefficient for the DCMD process is nearly the same over the wide range of operating temperature difference.

Effect of Vapor Pressure Difference on Produced Water Flux

Vapor pressure can be obtained from the mathematical modeling done previously. The transmembrane vapor pressure difference is derived thereafter. Since driving force of the mass transfer in DCMD is generated vapor pressure, caused by temperature difference, the transmembrane vapor pressure controls the generation of permeate water. The behavior of produced water flux with vapor pressure difference has been shown in Figure 19.

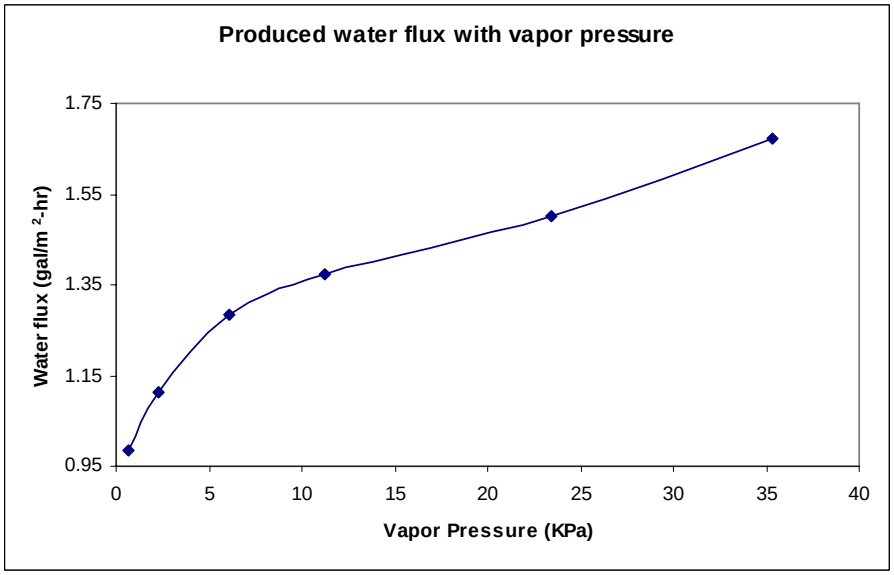

Figure 19. Produced Water Flux with Vapor Pressure Difference

Vapor Pressure Polarization Coefficient (VPC)

Like temperature polarization, the vapor pressure polarization also needs to be reduced to obtain an efficient membrane distillation process. In Figure 20, the nature of VPC with the bulk temperature difference has been shown.

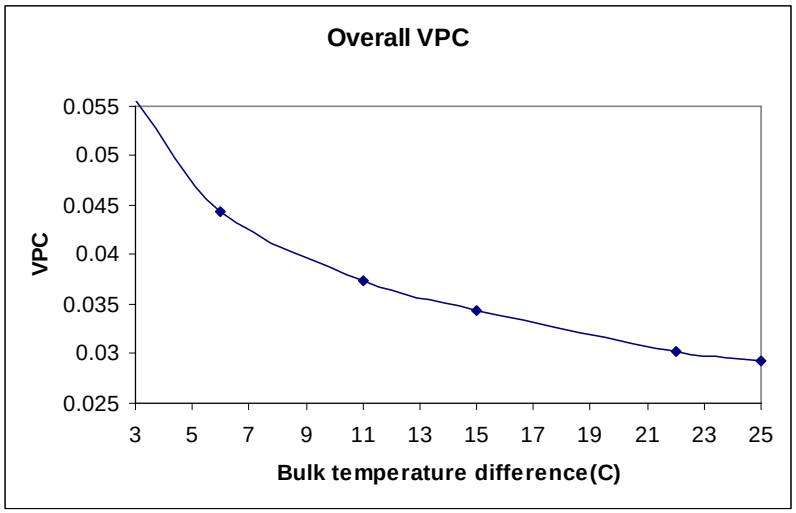

Figure 20. Overall VPC with Bulk Temperature Difference

Figure 21 indicates that overall VPC is decreasing gradually with the increase of the bulk temperature difference, and the value of VPC will remain in the range of 0.03 – 0.06, which is the sign of an extremely efficient DCMD process.

Membrane Distillation Coefficient (MDC)

The membrane distillation coefficient has been determined by using the model and calculations done previously. Behavior of MDC with average membrane pore temperature difference has been shown in Figure 21.

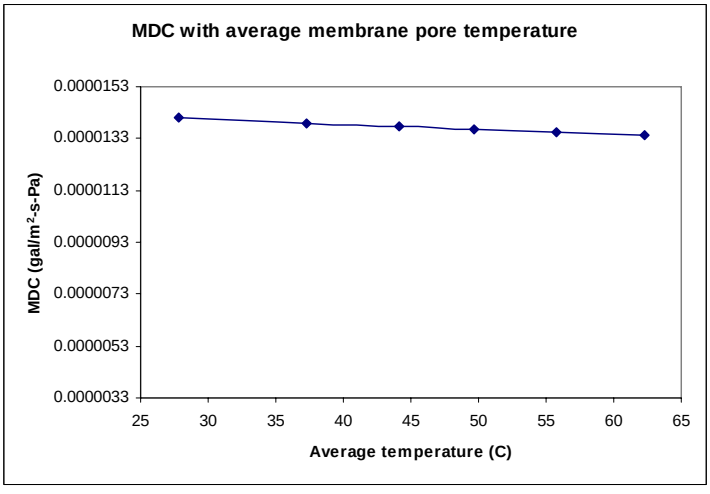

Figure 21. MDC with Average Membrane Pore Temperature

Figure 21 shows that the membrane distillation coefficient with average membrane pore temperature is nearly the same over a wide range of temperatures.

Comparison between Modeling and Experimental Results

Mass flux has been calculated both from the experiment and modeling and from the Figure 22 below. It can be said that theoretical and experimentally obtained mass fluxes approach nearly in the same way.

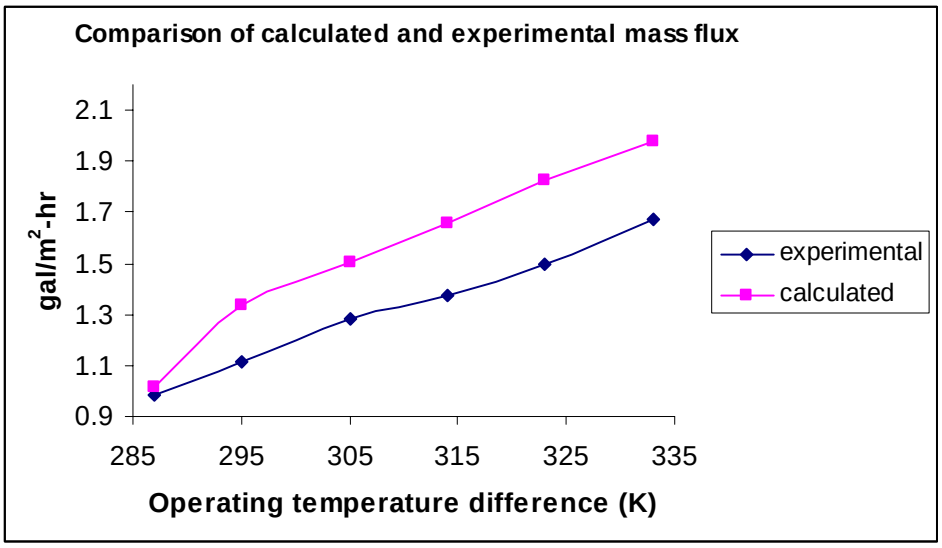

Figure 22. Comparison of Calculated and Experimental Mass Flux

From the discussion, it can be said that by increasing the operating temperature difference between the hot feed and cold feed, the produced permeate water flux will increase. The produced water flux is directly related to the operating temperature difference. With increasing the temperature difference, the heat transfer coefficient also should be increased or be nearly the same, which has been shown by modeling calculations. Also, the vapor pressure difference will be a direct function of temperature difference. Therefore, theoretically and by experiment, it can be said that by increasing the temperature difference, the vapor pressure difference will increase to produce permeate. This result has been obtained from the vapor pressure calculation in the modeling part. So the results obtained from experiment as well as from modeling are consistent. Also, the reducing nature of the graphs of temperature polarization coefficient and vapor pressure polarization coefficient gave an impression of a highly effective process. The experimental behavior and the behavior of derived data from the modeling are consistent.

CONCLUSION

It was found from the experimental studies that the Sunearth® flat solar collector has the highest solar to thermal conversion efficiency (~70%) and the homemade parabolic solar collector has the lowest solar to thermal conversion efficiency (5%).

A novel experimental setup has been installed by employing the hollow fiber membrane module. A complete theoretical modeling for heat and mass transfer phenomena is derived and various experimental data have been investigated and analyzed. Experiments were performed to determine the permeate water flux. Then various process parameters were calculated on the basis of the derived modeling, such as temperature polarization coefficient (TPC), overall heat transfer coefficient, vapor pressure polarization coefficient (VPC), membrane distillation coefficient (MDC), and permeate water flux. Through all these measured parameters, process efficiency was well understood. The calculated value of overall TPC here remained in the range of 0.04 to 0.06, and VPC remained in the range of 0.03 to 0.055. Since vapor pressure gradient, caused by temperature gradient, is the main driving force of the process, TPC and VPC should behave similarly in a decreasing way for an effective and efficient process. The graph discussed above represents the same trend for this process. The calculated overall heat transfer coefficient shows a nearly constant value (decreasing slightly) over the process. The membrane distillation coefficient graph has a decreasing trend, but nearly constant values prevail over the whole process. There was a similar pattern of calculated and experimental permeate mass flux. Those above explanations of parameters gave an impression that the DCMD process in this experiment is effective and efficient.

SYMBOLS

$a(x,T)$ = The water activity in the salt aqueous solution
$C(x)$ = Membrane distillation coefficient (MDC) (gal/m^2•s•Pa)
C_b = Global MDC
D = Diffusion coefficient of water vapor in air (m^2/s)
D_d = The diffusion coefficient of water vapor in air
d_h = Equivalent diameter of the flow channel (m)
D_k = Knudsen diffusion coefficient of water
h_c = Cold side heat transfer coefficient (W/m^2°K)
h_f = Heat transfer coefficient at hot side (W/m^2°K)
k = Thermal conductivity (W/m°K)
k_B = Boltzmann constant (J/K).
Kg = Conductivity of air (W/m°K)
Ks = Conductivity of the membrane material (W/m°K)
L = Module length (m)
M = Molecular weight of water, g/mol
Nu = Nusselt number
P = Total pressure inside the pores
$p_1(T_1)$, $p_2(T_2)$ = Vapor pressure of water at the membrane surface
P_a = Air pressure entrapped in the pores

p_m = Vapor pressure of water at membrane, (Pa)
Pr = Prandtl number
P_v^0 (T) = Vapor pressure of distilled water
ΔP_v = Transmembrane vapor pressure difference
R = Gas constant, J/mol•kK
r = Membrane pore radius
Re = Reynolds number
T_1 = Interfacial feed temperature (K)
T_2 = Interfacial permeate temperature (K)
T_{av} = Average temperature along the pores (K)
T_c = Bulk permeate temperature (K)
T_f = Bulk feed temperature (K)
T_m = Temperature at the membrane module (K)

τ = Temperature polarization coefficient
τ_c = Temperature polarization coefficient corresponding to permeate
τ_f = Temperature polarization coefficient corresponding to feed
δ = Thickness of membrane (30 μm)
ε = Membrane porosity
η = Vapor pressure polarization coefficient
η_a = Viscosity of vapor-air mixture (Pa•s)
η_c = Vapor pressure polarization coefficient in the permeate
η_f = Vapor pressure polarization coefficient in the feed
λ = Latent heat of water (kJ/kg)
ρ = Liquid density
τ = Membrane tortuosity

REFERENCES

[1] Lawson K.W. and Lloyd D.R., Membrane distillation. II. Direct contact MD, Journal of Membrane Science, 120 (1996) 123-133.

[2] Diez M.L., et al, Study of evaporation efficiency in membrane distillation, Desalination, 126 (1999) 193-198.

[3] Lagana, F., Barbieri, G., and Drioli, E., Direct contact membrane distillation: modeling and concentration experiments, Journal of Membrane Science**,** 166 (2000) 1-11.

[4] Abu Al-Rub, F.A., Banat, F., and Beni-Melhim, K., Parametric sensitivity analysis of direct contact membrane distillation, Separation Science and Technology**,** 37(14) (2002) 3245-3271.

[5] Ding Z., Ma, R., and Fane, A.G., A new model for mass transfer in direct contact membrane distillation, Desalination, 151 (2002) 217-227.

[6] Khayet, M., Godino, M. P., and Mengual, J.I., Study of asymmetric polarization in direct contact membrane distillation, Separation Science and Technology, 39(1) (2004) 125-147.

[7] Cath T.Y., Adams, V.D., and Childress, A.E., Experimental study of desalination using direct contact membrane distillation: a new approach to flux enhancement, Journal of Membrane Science**,** 228 (2004) 5-16.

[8] Khayet, M.,Velazquez, A., and Mengual, J.I., Modeling of mass transport through a porous partition: Effect of pore size distribution, Non-Equilib. Thermodynamics, 29 (2004) 279-299.

[9] Rodriguez-Maroto, J.M., and Martinez, L., Bulk and measured temperatures in direct contact membrane distillation, Journal of Membrane Science, 250 (2005) 141-149.

[10] Korngold, E., Korin, E., and Ladizhensky, I., Water desalination by pervaporation with hollow fiber membranes, Desalination, 107 (1996) 121-129.

[11] Gujit, M.C., Racz, I.G., Reith, T., and Hann, A.B., Determination of membrane properties for use in the modeling of a membrane distillation module, Desalination, 132 (2000) 255-261.

[12] Kim, J.J., Jang, T.S., Kwon, Y.D., et al, Structural study of microporous polypropylene hollow fiber membrane made by the melt spinning and cold – stretching method, Journal of Membrane Science**,** 93 (1994) 209-215.

[13] Dindore, V.Y., Cents, A.H.G., Brilman, W.F., and Versteeg, G.F., Shell-side dispersion coefficients in a rectangular cross-flow hollow fiber membrane module, Chemical Engineering Research and Design, 83(A3) (2005) 317-325.

[14] Sirkar, K.K., and Li, B., Novel membrane and device for direct contact membrane distillation-based desalination process, Industrial Engineering Chemical Research, 43 (2004) 5300-5309.

[15] Drioli, E., and Curcio, E., Perspectives for membrane contactors application in water treatment, Industrial Engineering Chemical Research**,** 10(1) (2004) 24-32.

[16] Khayet, M., Mengual, J.I., and Matsuura, T., Porous hydrophobic/ hydrophilic composite membranes: Application is desalination using direct contact membrane distillation, Journal of Membrane Science, 252 (2005) 101-113.

[17] Baudot, A., Floury, J., and Smorenburg, H.E., Liquid-liquid extraction of aroma compounds with hollow fiber contactor, AIChE Journal, 47(8) (2001) 1780-1793.
[18] Bird, R.B., Stewart, W.E., and Lightfoot, E.N., Transport Phenomena, Wiley, New York: 1960.
[19] Kreith, F., and Bohn, M.S., Forced convection over exterior surfaces, Principle of Heat transfer 5th Ed; PWS publish. Comp; Boston: 1997, 445-497.